Journal of Catalysis 264 (2009) 104–116

Contents lists available at ScienceDirect

Journal of Catalysis

journal homepage: www.elsevier.com/locate/jcat

Adsorption and reactivity of nitrogen oxides (NO_2, NO, N_2O) on Fe–zeolites

Mickaël Rivallan [a,b,c,*], Gabriele Ricchiardi [a,b], Silvia Bordiga [a,b], Adriano Zecchina [a,b,*]

[a] Università di Torino, Dipartimento di Chimica Inorganica, Chimica Fisica e Chimica dei Materiali, Via P. Giuria 7, 10125 Torino, Italy
[b] NIS Centre of Excellence, University of Torino, Italy
[c] Laboratoire Catalyse et Spectrochimie, ENSICAEN, Université de Caen, CNRS, 6 Bd Maréchal Juin, F-14050 Caen, France

ARTICLE INFO

Article history:
Received 29 November 2008
Revised 11 March 2009
Accepted 19 March 2009
Available online 26 April 2009

Keywords:
N_2O decomposition
Fe–zeolite
MFI
N_2O, NO, and NO_2 probe molecules
Fe(II) active sites

ABSTRACT

Nitrous oxide decomposition and temperature programmed desorption tests on Fe–ZSM-5 and Fe–silicalite show that the catalytic conversion mechanism of N_2O into N_2 and O_2 over Fe–zeolites is more complex than expected. Nitrogen oxides are formed as byproducts of the catalytic process with the major part consisting in NO_2 species adsorbed on the iron sites. FTIR spectroscopy of adsorbed N_2O, NO, and NO_2 has been used to investigate the structure and environment of the iron active species of the Fe–MFI catalysts before and after atomic oxygen deposition. The interactions of NO and N_2O probes on activated Fe–ZSM-5 have evidenced two families of mononuclear Fe(II) centers (Fe_A and Fe_B) differing in the coordination state of Fe. N_2O also interacts with Brønsted sites of Fe–ZSM-5 via hydrogen bonding. This type of interaction is nearly absent in Fe–silicalite. Polynuclear species (clusters) and iron oxide particles, whose concentrations are strongly influenced by the iron content and by the preparation methods are also present. When oxidized samples (by N_2O) are considered, the ability of Fe_A and Fe_B centers to adsorb N_2O and NO is strongly depressed. On the contrary, the surface chemistry of iron particles is not appreciably influenced. These results represent an indirect proof of the preferential presence of adsorbed oxygen on isolated Fe centers. NO titration of oxidized Fe–ZSM-5 results in the formation of a complex network of interplaying neutral (NO, NO_2, N_2O_4) and ionic species (NO^+, NO_2^-, NO_3^-). The cooperation of sites between Brønsted and iron active sites is demonstrated. The last observation is fully confirmed by the experiments performed using NO_2 probe that titrates both Brønsted and iron sites.

On the basis of the comparison of catalytic results of N_2O decomposition and of spectroscopic results concerning the titration of surface sites with N_2O, NO, and NO_2 obtained on the same samples (which form the main scope of the paper), it clearly emerges that mononuclear sites characterized by lowest coordination are the most active in N_2O decomposition. Under the adopted conditions, low or negligible activity is shown by Fe_xO_y clusters and Fe_2O_3 particles.

1. Introduction

The control of N_2O emissions is part of the efforts taken to limit greenhouse gas emissions [1], as dictated by the Kyoto Protocol. In fact despite its relatively small concentration in the atmosphere, nitrous oxide is the third largest greenhouse gas contributor to overall global warming, behind carbon dioxide and methane and attacks ozone in the stratosphere, aggravating the excess amount of UV light striking the Earth's surface. N_2O is mainly emitted by agriculture (65%) [2], while industrial sources, including the production of nylon [3] and nitric acid [4], and the burning of fossil fuel in internal combustion engines [5,6] are responsible for about 20% of total N_2O emissions. All these detrimental effects have led to the research on the development of efficient and stable de-N_2O catalysts. Among the many different de-N_2O catalysts proposed so far (mainly M–zeolites (M = Cu, Co, Fe, etc. [7]), perovskite-like mixed oxides [8] and precious metals supported (Pd, Rh, etc. [9]), we report here on Fe–MFI. This reaction first reported by Panov et al. [10,11] has also been proposed for the titration of surface active sites [12–26]. It is generally accepted that surface iron species form the core of the catalytic site, and that the mechanisms of N_2O decomposition likely pass through an adsorbed oxygen intermediate called "α-oxygen" [10]. The most frequently proposed mechanisms in direct N_2O decomposition are

(a) $N_2O + (*) \rightarrow N_2 + {}_*O$
$N_2O + {}_*O \rightarrow N_2 + O_*O$
$O_*O \rightarrow O_2 + (*)$ see [17]
(b) $2N_2O + 2(*) \rightarrow 2N_2 + 2_*O$
$2_*O \rightarrow O_2 + 2(*)$ see [15,22]
(c) $N_2O + (*) \rightarrow N_2 + {}_*O$

* Corresponding authors. Address: Università di Torino, Dipartimento di Chimica Inorganica, Chimica Fisica e Chimica dei Materiali, Via P. Giuria 7, 10125 Torino, Italy.
E-mail addresses: Mickael.rivallan@ensicaen.fr (M. Rivallan), Adriano.zecchina@unito.it (A. Zecchina).

0021-9517/$ - see front matter © 2009 Elsevier Inc. All rights reserved.
doi:10.1016/j.jcat.2009.03.012

$N_2O + {}_*O \rightarrow N_2 + {}_*O_2$
$N_2O + {}_*O_2 \rightarrow N_2 + {}_*O_3$
${}_*O_3 \rightarrow {}_*O + O_2$ see [27]

In mechanism (b) (Langmuir–Hinshelwood mechanism), the migration of oxygen from one active site (∗) followed by recombination with another oxidized site is the rate-determining step [15,22]. This reaction mechanism needs the active participation of at least two iron centers that are not necessarily located in adjacent positions. In mechanisms (a) [17] and (c) [27] (Eley–Rideal mechanisms), N_2O decomposition and oxygen evolution occur at the same isolated sites (∗) after successive collisions between N_2O with (∗) and ${}_*O$ for (a), and with (∗), ${}_*O$, and ${}_*O_2$ for (c). The above described mechanisms are all in agreement with transient response experiments, showing that N_2 appears before O_2 upon direct N_2O decomposition pulses in the 773 to 848 K interval. This is because in all cases the global decomposition reaction is limited by the reactions steps leading to O_2 gas phase. More recent accurate temporal analysis of products [17] strongly suggests that mechanism (a) is the most likely. From the point of view of the oxygen species formed on iron active sites (∗), the three mechanisms are associated with increasingly complex oxygen species: ${}_*O$, O_*O, and ${}_*O_2$ for (a); ${}_*O$ for (b); and ${}_*O$, ${}_*O_2$, and ${}_*O_3$ for (c). Other very relevant results resulting from these catalytic experiments are

(a) Fe–ZSM-5 is always more active than Fe–silicalite containing the same amount of Fe [17,22–24]; from this important point, the role of Al in catalytic process is inferred. Some authors have proposed interesting Fe–Al configurations on the basis of theoretical models [28], or contributions of Al in N_2O interaction [29,30];
(b) The active sites are formed during activation in inert atmosphere or in vacuo [17,22–24]. There is a widespread agreement that after this treatment a large fraction of iron is in extra-framework position and in the divalent state;
(c) The fraction of active sites present depends upon many factors (impregnation methods, Fe concentration, and H_2O residual pressure). An analysis of the data published so far suggests that the samples can be quite heterogeneous [31];
(d) The fraction of clusters Fe_xO_y and the Fe^{2+}/Fe^{3+} ratio after activation are also very much influenced by the sample history;
(e) The activity augments with increasing activation temperature in inert gas; the same implies for the number of active sites [17,22–24];
(f) At low Fe content, the number of Fe sites where adsorbed oxygen species are formed is roughly identical in Fe–ZSM-5 and Fe–silicalite [17,22–24];
(g) The activity (calculated per Fe center) increases with dilution [22]. The fraction of active sites (calculated with respect to the total amount of introduced iron) can reach about 35% for the most diluted samples (<1000 ppm). It can be so concluded that the active sites contain a very small number of Fe atoms or, more likely, a single atom. From the above considerations it is also inferred that clustered species, becoming relevant at the highest Fe contents, are characterized by lower or negligible catalytic activity in N_2O decomposition. The debate concerning the nuclearity of the catalytic sites (mono or di-nuclear) continues.
(h) The number of "α-sites" (i.e. the Fe sites where atomic oxygen can be deposited during N_2O decomposition) grows with the Fe concentration, this growth being, however, definitely smaller than that of clustered species as expected by considering the atomic dispersion of the active sites [32].
(i) All other factors being equal, the number of active sites is maximum on catalysts formed by high temperature activation of isomorphously substituted zeolites [22], as compared, for example, with catalysts obtained with post-synthesis impregnation.

An interesting point concerning the mechanism of N_2O decomposition reaction is the positive effect of NO [33–39], which enhances the decomposition rate of N_2O. The last observation has relevant mechanistic implications and has recently animated the debate since recent papers have reported on the presence of NO_y species presumably formed on the Fe–ZSM-5 during the first catalytic steps [33,38,40,41]. This problem will be specifically addressed in the discussion of the results obtained using NO_2 probe.

As for the structure of active sites, the crystalline character of the hosting matrix (MFI framework) has spread the conviction that the structure is characterized not only by extremely low nuclearity but also by well-defined geometry. This conviction, which at first sight establishes an analogy with iron-based homogeneous catalysts and enzymes, has conferred a unique model character to this catalyst and has stimulated a great deal of investigations based on accurate catalytic measurements and on physical characterization methods. The results of this intensive research work have been recently reviewed [31]. From the comparison of whole set of experimental and theoretical results, it has been concluded that despite the crystalline character of the hosting matrix, the structure of iron sites of Fe–MFI systems is less defined than initially hypothesized and that the analogies with Fe-based enzymatic systems must be cut down to size.

As for the characterization with physical methods, the whole set of spectroscopic techniques has been used including FTIR of adsorbed molecules, UV–Vis-NIR, XANES, and EXAFS. In particular, the following facts have been firmly established:

(a) After severe thermal treatment, the Fe^{3+} originally located in the framework position (isomorphously substituted Fe–ZSM-5 and Fe–silicalite) migrates in extra-framework positions (isolated and/or clusters) and undergoes reduction to Fe(II). These sites are highly coordinatively unsaturated and are able to interact with many adsorbates. To a first approximation the isolated sites can be considered as Fe(II) ions linked to the framework via two strong bonds as reported for Co^{2+} ions in Co–ZSM-5 [42] and for Cr supported on silica [43,44]. In the first coordination sphere of Fe(II) ions, a variable number of weaker ligands (oxygen of adjacent SiOSi groups) can be present whose number depends upon the location of Fe(II) ions on the surface of the MFI structure. A representation of the structure of isolated species sites is illustrated in Scheme 1.In the model structure reported in Scheme 1 (valid only for Fe–ZSM-5), Fe^{2+} substitutes two cationic sites (like in β sites of Ref. [42]). The scope of this picture is simply to show that in the coordination sphere of Fe^{2+}, strong and weak coordination ligands are clearly present. This model has only qualitative character and cannot be extended to Fe–silicalite, because in this case no trivalent ions are present in the structure after the thermal treatments. In this case the Fe^{2+} ions are really grafted to the siliceous framework via two strong FeOSi bonds (like in the Cr/SiO_2 system). Considering the first coordination sphere, the structure of all iron centers (either on Fe–ZSM-5 or on Fe–silicalite) can be schematized with a common formula FeL_nX_m (where $n \geqslant 2$, $m \geqslant 2$).
(b) The spectra of adsorbed NO on isomorphously substituted Fe–ZSM-5 and Fe–silicalite treated at 773 K are very similar: NO interacts with isolated Fe^{2+} centers with the formation of tri-nitrosylic and di-nitrosylic complexes whose frequencies are slightly higher for Al-containing samples (suggesting the presence of Al close to Fe site) [31]. Furthermore, the inten-

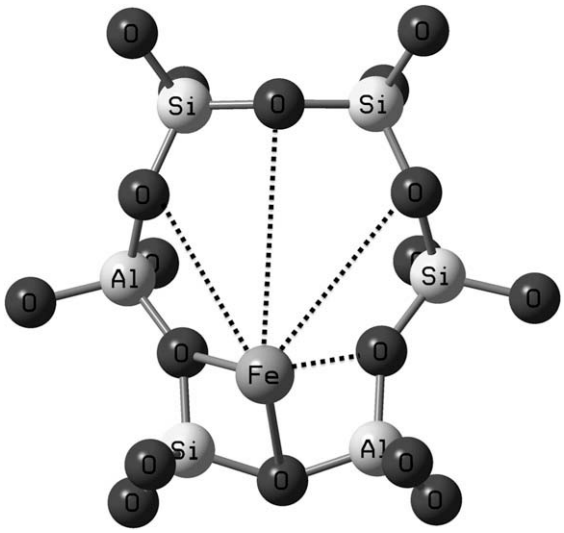

Scheme 1. FeL_nX_m (with $n \geqslant 2$, $m \geqslant 2$), where L is an O atom in SiOAl, whereas *X* corresponds to an O atom in SiOSi.

sity of the NO peaks is higher on Al-containing samples. It means that Al helps in Fe dispersion and hence increases the abundance of mononuclear or low nuclearity Fe species.

(c) The predominance of extra-framework species is *a fortiori* verified in samples prepared by wet or gas phase impregnation, because in these cases Fe is in extra-framework position already obtained from the preparation step. From the concise description illustrated above, few well-ascertained facts and few remaining problems are emerging. Among the ascertained facts, the extra-framework character and the reduced valence state of isolated iron centers must be mentioned. Among the problems, the exact nuclearity, the detailed structure of the active sites, the role of Al, and the potential role of NO_x intermediates in N_2O decomposition, and their location must be recalled. In the present work, the N_2O decomposition on Fe–ZSM-5 and Fe–silicalite is discussed and compared. This comparison is necessary in order to investigate the role of Al on the catalytic activity. N_2O Temperature Programmed Reaction (TPR) and Temperature Programmed Desorption (TPD) experiments form the core of the catalytic tests section. A second section devoted to FTIR characterization consists in the use of N_2O, NO, and NO_2 probes, with the scope to investigate the structure and nuclearity of the iron active centers. The NO_2 probe has also been used to probe pure H–ZSM-5 and silicalite.

2. Experimental

2.1. Sample preparation

Fe-exchanged ZSM-5 zeolites were prepared using aqueous ion-exchange [45]. The parent zeolite, NH_4-ZSM-5 (nominally Si/Al = 15, 40, 140; Na_2O = 0.05 wt.%), was supplied by Zeolyst International. For the aqueous ion-exchange, 0.3 g of NH_4-ZSM-5 was added under stirring in two recipients, each one containing a 5-ml 0.01 M iron(III) oxalate solution. The solution of iron(III) oxalate was prepared using $Fe_2(C_2O_4)_3 \cdot 6\,H_2O$ (99%, Aldrich) and deionized water. After 24 h the mixtures were filtered, washed with deionized water, dried in atmosphere, and used for further investigations. During the impregnation, the ferric oxalate solution and the zeolite slurries were carefully kept away from light. Here, the sample prepared by the oxalate method will be referred to as Fe–Z-*x*, where *x* corresponds to Si/Al ratio. The Fe–silicalite catalyst (Fe–S) was prepared following the hydrothermal method described in detail by Ratnasamy and Kumar [46]. Briefly, the Fe–silicalite catalyst was obtained by mixing solutions of oxalic acid, ferric nitrate, sodium silicate, and tetrapropyl-ammonium bromide. The so-obtained gel was crystallized in a tumbling autoclave at 440 K for 4 days. The so-obtained solid was separated, washed, dried, and calcined in air at 823 K. With the aim of removing any undesired extra-framework cations coming from the reagents, the solid was then ion-exchanged with 1 M NH_4NO_3 solution and dried. The estimated Fe content is approximately 1.0 wt.%. Pure silicalite was furnished by ENI Tecnologie Laboratories (S. Donato Milanese). Chemical composition was determined by elemental analysis, by means of a Varian Vista Pro Axial ICP spectrometer. Fe-standard solutions were made from Spectrascan-standard (1000 ppm) delivered by Teknolab.

2.2. Catalytic activity tests

Catalyst activity tests were performed using an integrated quartz micro-reactor and mass spectrometer system (CATLAB from Hiden). The system features a fast-response, low thermal mass furnace with integrated air-cooling, a precision Quadrupole Mass Spectrometer, and a quartz inert capillary with "hot zone" inlet for continuous close-coupled catalyst sampling with minimal dead volume and memory effects. The in-bed thermocouple ensures optimal measurement of catalyst temperature. The reactant gases are supplied through electronic mass flow controllers. An amount of 200 mg pelletized catalyst (particles size 250 to 500 μm) diluted in the same volume of mesh size of α-Alumina (Talum) is held between plugs of quartz wool in a quartz tubular vertical flow reactor (Ø = 5 mm). The pre-treatment of the catalyst is realized at 773 K (ramp temperature of 5 K min^{-1}) under He:Ar mixture (99:1 vol.%) with a flow of 100 cm^3 min^{-1}. After 2 h the reactor is cooled down to 300 K in He:Ar. Then the N_2O decomposition test (TPR) is performed from 300 K to 773 K (5 K min^{-1}), with a gas mixture of He: N_2O:Ar (94:5:1 vol.%) kept at a constant flow of 100 cm^3 min^{-1}. Fig. 1 shows the typical catalytic test done over Fe–MFI samples. The whole catalytic test starts with a 2-h activation treatment at 773 K followed by a first TPR from RT to 773 K. Afterwards the sample is reactivated up to 773 K in He and a second TPR is performed.

Temperature Programmed Desorption (TPD) has been performed between the two TPR cycles (time range 550 to 650 min (Fig. 1)) under inert He:Ar (99:1 vol.%) atmosphere (100 cm^3 min^{-1}) over Fe–MFI previously N_2O treated from RT to 773 K (5 K min^{-1}). Isotherm tests have also been performed at T = 623, 673, and 723 K over Fe–Z-40 freshly activated at 773 K for 2 h. The reactant gas was composed of N_2O (5 vol.%) in a constant flow of 100 cm^3 min^{-1} completed by He:Ar (99:1 vol.%). During these catalytic and desorption tests, the following AMU: 28 (N_2), 30

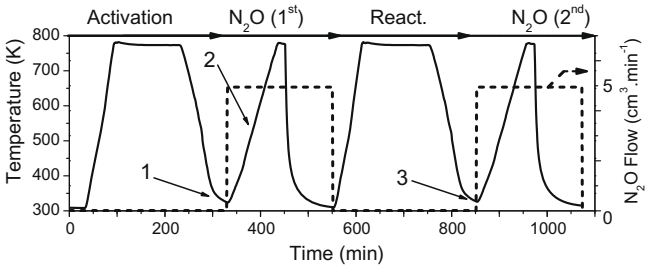

Fig. 1. Scheme of the whole catalytic test done over Fe–MFI. Temperature (black line) and N_2O flow (dotted line) are plotted as a function of time.

(NO), 32 (O_2), 40 (Ar), 44 (N_2O), and 46 (NO_2) m/e have been collected simultaneously by the Quadrupole Mass Spectrometer. For N_2 and NO, the contributions due to N_2O cracking fragments (m/e = 28 and 30) have been subtracted.

2.3. FTIR characterization

The IR experiments were performed on a Bruker IFS 66 FTIR instrument equipped with a cryogenic MCT detector and run at 2 cm^{-1} resolution. All the samples under study were in the form of self-supporting pellets suitable for measurements in the transmission mode.

N_2O adsorption and subsequent desorption experiments were performed at RT. The desorption trends have also been investigated for samples previously contacted with N_2O at 573 K. In both cases the sequence of IR spectra was recorded at RT by gradually reducing the N_2O equilibrium pressure in the cell until $P_{N_2O} = 10^{-3}$ Torr.

The IR spectra of adsorbed NO have been performed on

(i) activated samples under vacuum for 2 h at 773 K (Fe–Z-*x* and Fe–S);
(ii) samples pre-treated in N_2O for 1 h at 573 K (Fe–Z-*x* and Fe–S);
(iii) reactivated samples in vacuum for 2 h at 773 K (Fe–Z-40); corresponding to steps 1, 2, and 3 of Fig. 1, respectively.

After NO admission the evolution of the spectra with time was followed by IR (not reported). After 30 min contact a sequence of IR spectra was recorded by gradually reducing the NO equilibrium pressure in the cell until $P_{NO} = 10^{-3}$ Torr. The intensity of the NO spectra was "normalized" using invariant lattice modes of the zeolite as reference. The IR results of NO titration are usually quite reproducible, because the same bands are observed in all cases. The relative intensity of the bands, however, can moderately vary from one experiment to the other. This variation is always very small when the same thermal treatments are performed.

The IR spectra of NO_2 adsorption and subsequent desorption experiments were performed at RT on Fe–ZSM-5, Fe–silicalite, H–ZSM-5, and silicalite outgassed at 773 K. In all cases 40 Torr of NO_2 was allowed to contact the sample: afterwards a sequence of IR spectra was recorded at RT by gradually reducing the NO_2 equilibrium pressure in the cell until $P_{NO_2} = 10^{-3}$ Torr. The intensity of the NO_2 spectra was "normalized" using invariant lattice modes of the zeolite as reference.

3. Catalytic tests

3.1. N_2O-TPR

The N_2O decomposition was studied in the quartz micro-reactor and Mass Spectrometer system. The scope was to determine the onset temperature (T_{onset}) of the reaction and of presumed "α-oxygen" formation on Fe–MFI activated at 773 K. Two TPRs have been performed on each Fe–MFI catalysts with diverse Al content (Si/Al ratios 15, 40, and 140) and on an Al-free Fe–silicalite sample (Si/Al = ∞) (Fig. 2).

On Fe–Z-15 and Fe–Z-40 the first cycle of N_2O decomposition starts at very low temperature (550 K). These catalysts exhibit also a loss of activity in the 600 to 670 K range. Afterwards their catalytic ability is recovered and total conversion is reached at 720 and 775 K for Fe–Z-40 and Fe–Z-15, respectively. We can also remark that Fe–S presents also a very modest inflection of activity curve at 750 K. During the second TPR performed on reactivated Fe–Z-40 samples (2 h at 773 K in He inert flow), the total conversion is achieved at 650 K, i.e. at a temperature distinctly lower than those usually reported in the literature. As for the sample with very low Fe content (Fe–Z-140), the different N_2O cycles give similar results and the activity is always poor.

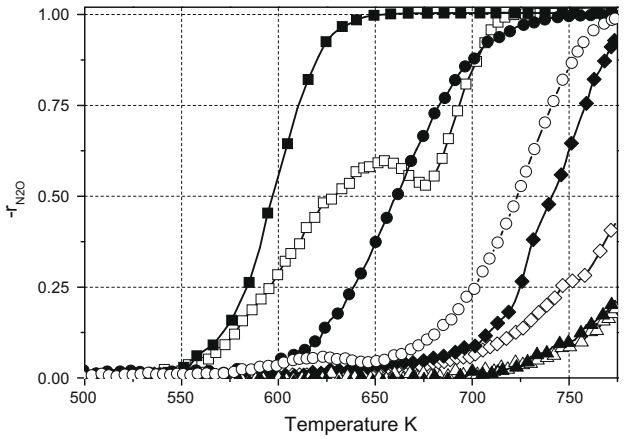

Fig. 2. Fractional conversion of N_2O as a function of reaction temperature over freshly activated and reactivated Fe–ZSM-5 (open and full symbols, respectively): Fe–Z-15 (-●-), Fe–Z-40 (-■-), and Fe–Z-140 (-▲-). The N_2O decomposition on Al-free Fe–S (-♦-) is reported for comparison.

The loss of activity in the 600 to 670 K range which appears during the first cycle has been already discussed in the past and has been interpreted as due to an auto-reduction of Fe^{3+} to Fe^{2+} favored by the high Al content [47]. We prefer to consider this feature as associated with a structural change of the iron active sites associated with the initial oxidation reaction steps. During the second TPR, we do not observe any loss of activity, some structural change of the active sites have occurred during the first catalytic cycle. Fe–Z-140 does not exhibit this trend, probably due to the low iron incorporated during synthesis (i.e. low Fe active sites content).

In more detail, for a given sample (containing a certain concentration of active sites) and at constant N_2O pressure, the disappearance rate of N_2O ($-r_{N_2O}$) at constant P_{N_2O} in the reaction (1) is only dependent upon the temperature through the equation: $(-r_{N_2O}) \alpha k$, with $k = k_0 \cdot e^{-Ea/RT}$.

$$2N_2O \rightarrow 2N_2 + O_2 \quad (1)$$

The activation energy (Ea) is held between 145 ± 5 kJ mol^{-1} on all catalysts (Table 1) and appears substantially independent upon Fe and Al concentrations. In order to confirm this observation, data published so far in the literature [10,13,16,17,36,47–54] have been also displayed as function of the Fe and Al contents (Fig. 3a and b).

Considering the extremely large Fe concentration interval and the different history of the investigated samples, our conclusion concerning the independence of Ea upon Fe concentration is fully confirmed (all data are randomly scattered in the 150 ± 20 kJ mol^{-1} interval). This important result strongly suggests that (a) the same sites (or families of similar sites) are involved on all samples; (b) the sites do not belong to the Fe_xO_y clusters because in such cases the activation energy should depend upon the cluster size and hence upon iron concentration. These considerations are strongly in favor of the hypothesis that the active sites contain single Fe

Table 1
Chemical compositions and activation energies[a] of Fe–MFI catalysts.

Catalyst	Si/Al	Fe wt.%	Ea in kJ mol^{-1}
Fe–Z-15	15	0.37	147 ± 3
Fe–Z-40	40	0.32	150 ± 2
Fe–Z-140	140	0.18	142 ± 4
Fe–S	∞	1.0	144 ± 4

[a] From N_2O decomposition (TPR).

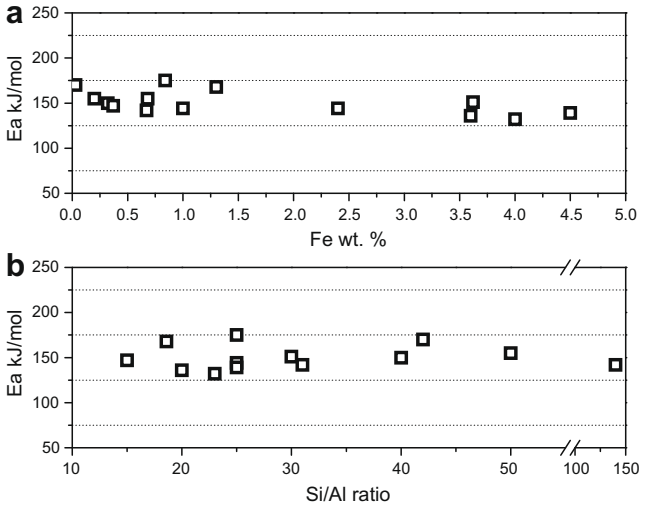

Fig. 3. (a) Influences of Fe content (0.03 < Fe wt.% < 5.0); and (b) Al (10 < Si/Al < 140) content, respectively, on Ea reported from Refs. [10,13,16,17,35,43–50].

centers implanted on the MFI matrix. Extremely small clusters (for instance dimers) are, however, not completely ruled out.

The Ea is also not appreciably influenced by Al concentration. This result is even more surprising, because Fe–ZSM-5 samples are known to be more active than Al-free Fe–silicalite samples. From this result it is evident that the higher activity derived from the presence of Al is not due to a substantial decrement of the Ea of the rate-determining step (which can be either the reactive N_2O collision with adsorbed $_*O$ or atomic oxygen $_*O$ recombination to form O_2).

3.2. Isotherms at 623, 673, and 723 K

In order to limit the parameters which must be considered during N_2O abatement, isotherm tests have been performed over Fe–Z-40 (Fe 0.32 wt.%) at 623 K (decomposition starts); 673 K (loss of activity) and 723 K (total decomposition) (Fig. 4).

Upon flowing N_2O (5 vol.%) on freshly activated Fe–Z-40 at 623 K, NO and N_2 traces appear first at the outlet of the reactor. After 10 min, NO starts to decrease while O_2 emerges. All these signals vanish after 1 h interaction. It implies that at this temperature, the catalytic products are covering (poisoning) the sites and that the decomposition does not proceed until O_2 desorption.

At 673 K, about 40% of N_2O is directly converted and only N_2 and O_2 products are detected. As the isotherm at 673 K proceeds, the activity of the catalyst decreases, because the N_2O decomposition products still accumulate (as before). The probable accumulation may consist of strongly adsorbed NO_y species. As after 10 h the catalyst loses about 80% of its initial activity (not shown), we may so conclude that the reaction (1) needs higher temperature to be sustained. This phenomenon can also explain the loss of activity observed during the first N_2O-TPR (Fig. 2). The full and stable conversion is reached at high temperature (T = 723 K), in fact after 20 h contact with N_2O (5 vol.%) the conversion remains unchanged, so confirming the high ability of Fe–Z-40 in direct N_2O decomposition.

The volumes of N_2, O_2, and NO detected in outlet reactor and the N_2O consumption during the first hour of isotherm at 623 K can give some clues about the species adsorbed on the catalysts. The ratio $V(N_{at})/V(O_{at})$ coming from the decomposition of native N_2O ($V(N_{at})/V(O_{at}) = 2$) is larger than that expected on the basis of the stoichiometry of reaction (1). This suggests that N atoms are released in higher quantity than O atoms and that oxygen is adsorbed on Fe–MFI catalyst. Whether this oxygen is an atomic species (α-oxygen) or a NO_y-like species (or both) is difficult to establish. The presence of NO in the outlet gas phase suggests that besides reaction (2) and dominant paths (a, b, and c) also the consecutive reaction (3) must be considered [40,41]:

$$N_2O + (*) \rightarrow N_2 + O_* \quad (2)$$

$$N_2O + O_* \rightarrow 2(NO)_* \rightarrow 2NO + (*) \quad (3)$$

In fact at 623 K, NO can also react with adsorbed oxygen, the formation of NO_2 (N_2O_4) and hence of surface nitrites and nitrates must be taken into consideration.

3.3. Temperature Programmed Desorption (TPD)

In order to shed light on the possible NO_y ad-species, TPD test was done. Fig. 5 displays the results obtained over Fe–Z-15 and Fe–Z-40 previously oxidized until 773 K and cooled down to RT under N_2O (5 vol.%).

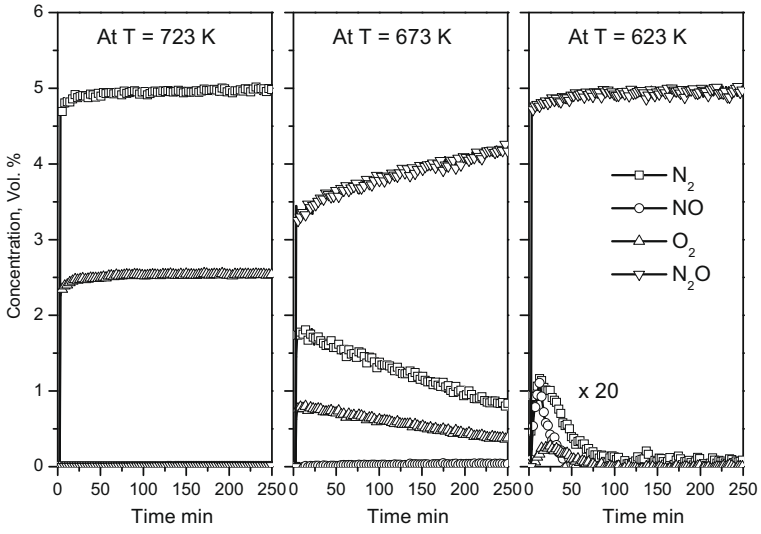

Fig. 4. Response curves of N_2, NO, O_2, and N_2O obtained at 723, 673, and 623 K after switching at t = 0 min from inert atmosphere (1% Ar, 99% He) to (5% N_2O, 1% Ar, 94% He) mixture over Fe–Z-40 previously activated.

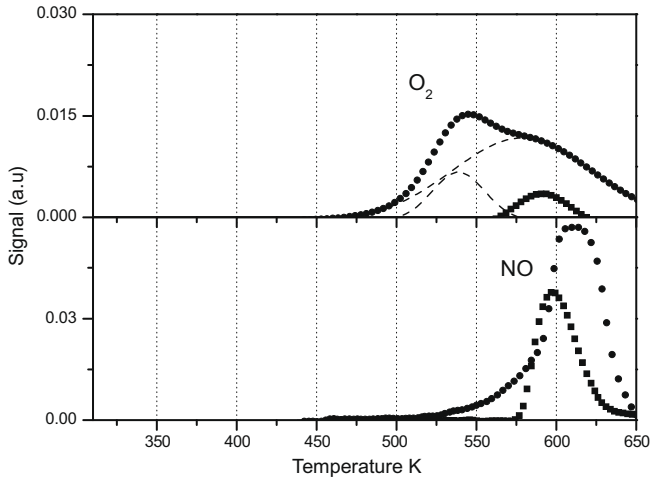

Fig. 5. Response curves of O_2 and NO obtained during Temperature Programmed Desorption (TPD) performed over Fe–Z-15 (-•-), Fe–Z-40 (-■-) previously N_2O-oxidized at 773 K.

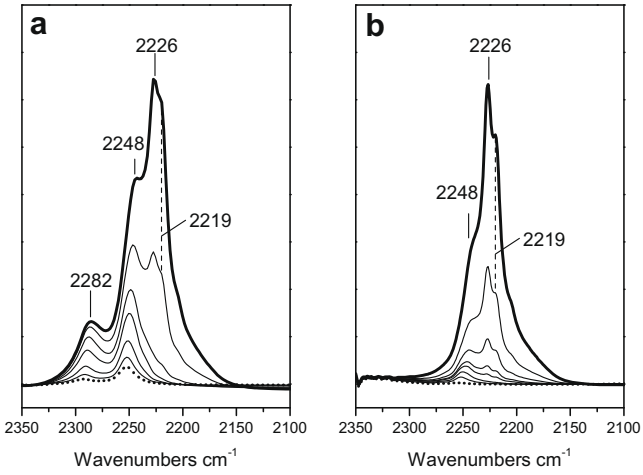

Fig. 6. FTIR spectra (background subtracted) of Fe–Z-40 freshly activated at 773 K in contact with N_2O at RT (a) and at 573 K (b) and following desorption at RT from $P_{N_2O} = 20$ Torr (bold line) to $P_{N_2O} = 10^{-3}$ Torr (dotted line).

Unlike Fe–silicalite and Fe–Z-140 (not shown), Fe–Z-15 and Fe–Z-40 exhibit two distinct TPD signals of O_2 and NO. The TPD of Fe–Z-15 shows two oxygen maxima as a result of the presence of two different families of iron adsorbing sites. The first oxygen release could come from recombination of species adsorbed on highly active sites (Langmuir–Hinshelwood), because it occurs at lower temperature (4). The second oxygen desorption occurring on both samples (Fe–Z-15 and Fe–Z-40) is probably the result of the decomposition of NO_x species (5) because it is coupled (and proportional) to NO signal:

$$2Fe(O_*) \rightarrow 2Fe(*) + O_2 \quad (4)$$

$$2Fe(NO_2) \rightarrow 2Fe(*) + 2NO + O_2 \quad (5)$$

The fact that Fe–Z-40 sample does not display the second O_2 signal at ~550 K is quite difficult to explain. We may tentatively suggest that on this catalyst characterized by highest activity reaction (3) is not occurring. In conclusion TPD test reveals the presence of NO_x products on the catalyst's surface after N_2O interaction (at 773 K) and that NO can be evolved in the gas phase. We have clear evidence that NO can participate as reactant in the complex network of reactions associated with the N_2O decomposition.

4. FTIR characterization using N_2O, NO, and NO_2 as probe molecules

4.1. Nitrous oxide

The IR spectra of N_2O adsorbed at RT on Fe–Z-40 freshly activated and pre-treated in N_2O at 573 K (oxygen deposition) are shown in Fig. 6a and b.

Upon adsorption of N_2O (20 Torr) on the sample activated at 773 K (under vacuum condition) a fraction of Brønsted acid Si(OH)Al groups are shifted from 3610 to 3470 cm^{-1} (not shown) because of the weak hydrogen-bonding interaction reported below

$$Si(OH)Al + N_2O \rightarrow Si(OH\cdots N_2O)Al \quad (6)$$

The silanols groups (peak at 3750 cm^{-1}) are not perturbed by N_2O adsorption at RT. The N_2O species weakly adsorbed on strong Brønsted sites is associated with an intense band with maximum at 2226 cm^{-1} due to the ν(N–N) stretching vibration. The ν(N–O) stretching vibration occurs at lower frequencies [55,56] and hence cannot be observed. The 2226 cm^{-1} band, also present on pure H–ZSM-5, quickly disappears upon outgassing at RT. N_2O interaction with pure silicalite (not shown), where only silanols are present, do not show formation of these weakly adsorbed precursor species. The additional band at 2282 cm^{-1} and the shoulder at 2248 cm^{-1} are less reversible upon outgassing and are ascribed to N_2O adsorbed on Fe sites [47].

$$Fe^{x+} + N_2O \rightarrow Fe^{x+}\cdots N_2O \quad (7)$$

Two different families of sites (Fe_A and Fe_B) are involved likely characterized by different coordinative situations (lower and higher, respectively). N_2O interaction on pre-oxidized catalyst (Fig. 6b) results in Fe_A and Fe_B sites behaving differently toward oxidation. In fact A sites are no more detected while B sites population appears only substantially weakened. This behavior can be explained as follows: (i) upon oxidation with N_2O at 573 K, A sites (2282 cm^{-1}) which are the most active become fully covered by oxygen species. Consequently they do not interact with N_2O probe; (ii) Fe_B sites, belonging to a less active family, are less affected. Formation of NO_x species could also partially deactivate Fe_A and Fe_B sites. The latter hypothesis cannot be discarded because the results of the catalytic tests obtained previously have shown that formation and subsequent decomposition of surface NO_2^- occur (5). It must be recalled that, if present, nitrites species are not detectable by FTIR because their characteristic spectral region falls in the 1440 to 1100 cm^{-1} range [57,58], where intense modes of the siliceous MFI matrix occur.

In conclusion the special character of the N_2O probe is not only associated to its ability to titrate different families of unsaturated Fe^{2+} sites, but also to its character of reactant in the investigated decomposition. It is quite conceivable that ($Fe^{2+}\cdots ON_2$) are the first intermediates in the oxidation step of the decomposition:

$$Fe^{2+} + N_2O \leftrightarrow Fe^{2+}\cdots ONN \rightarrow (FeO)^{2+} + N_2 \quad (8)$$

The higher concentration of adsorbed (hydrogen bonded) N_2O on Al-containing samples could partially contribute to explain the higher reactivity of these samples with respect to Al-free zeolites.

4.2. Nitric oxide

FTIR spectroscopy of adsorbed NO has been used by many authors in the past to explore iron sites dispersed in inorganic matrices, as testified by the rich literature reporting IR spectra of Fe-nitrosyl complexes in zeolites [35,59–62]. This method is based on the use of NO as a titrant of the exposed sites and is made pos-

sible by the well-known exceptional affinity of NO toward Fe^{2+} and Fe^{3+} centers, leading to a formation of $Fe^{x+}(NO)_n$ nitrosyls (n = 1, 2, 3) characterized by extremely intense IR bands. The high extinction coefficient of nitrosylic bands allows to probe samples containing very low concentration of Fe centers [31]. A useful feature of this method is also related to the fact that upon changing the NO equilibrium pressure, the full range of coverage can be explored. Under these conditions all surface centers are titrated.

The typical nitrosyl bands formed upon NO adsorption on the Fe–MFI sample, previously activated in vacuum at 773 K, are displayed in Fig. 7. The results illustrated in Fig. 7b–d are typical of diluted Fe–zeolites samples. They are similar to the results of Bell et al. (Si/Al = 25) [63] (even when prepared in a different way) and to the results obtained on samples obtained by activation of isomorphously substituted Fe–ZSM-5 and Fe–silicalite [31]. The spectrum reported in Fig. 7a is quite anomalous because it is characterized (beside the usual bands) by the presence of a prominent peak at 1880 cm^{-1} which is less evident on the other samples. This spectrum is illustrated here because it shows great similarity to the spectra reported by Lezcano et al. (Si/Al = 11) [64]. As reported in the literature [31,35,59–62] the assignment of the bands in the 1950 to 1725 cm^{-1} range is the following:

- the broad and asymmetric adsorption at 1880 cm^{-1}(particularly prominent on Fe–Z-15 (Fig. 7a), practically unperturbed by the decrease in P_{NO}, is assigned to $Fe^{3+}(NO)$ complexes mainly located on the surface of Fe_2O_3 clusters (because this band is preferentially observed on highly concentrated samples)
- the couple of bands at 1918 and 1810 cm^{-1}, gradually decreasing with NO pressure, is related to $Fe^{2+}(NO)_3$ complexes;
- the pair at 1845/1767 cm^{-1}, growing upon NO removal, is assigned to $Fe^{2+}(NO)_2$. These species are very stable and cannot be removed by outgassing at RT. This enhanced stability strongly suggests that the involved Fe(II) centers are the Fe_A sites (which are the most coordinatively unsaturated and hence are expected to bind more strongly NO).

As reported before (in N_2O titration), a second more highly coordinated iron species (Fe_B) is also present on the surface, which is also able to form tri-nitrosylic complexes. However, in this case nitrosyls are more weakly adsorbed and can be easily destroyed without any formation of di-nitrosylic intermediate upon decreasing the pressure (see for instance the spectra reported in Fig. 8a). A plausible explanation of this observation is that these Fe_B species have additional weak ligands (SiOSi or SiOAl) in the coordination sphere of Fe center and that the adsorption/desorption process is similar to a ligand displacement reaction. The total enthalpy of this reaction is smaller than that of A sites, because the contribution of NO adsorption/desorption is counterbalanced by the opposite contribution of the simultaneous ligand displacement. This situation is similar to that observed for Cr(II) grafted on silica, where analogous ligand displacement reactions have been observed upon CO and NO adsorption/desorption [43,44].

As already discussed by Zecchina et al. [31] the frequency of the NO stretching modes of the equivalent $Fe^{2+}(NO)_n$ complexes is statistically higher on Fe–ZSM-5 than on Fe–silicalite. This is mainly due to the statistical presence of Al in the first or second coordination sphere of anchored Fe^{2+}. This parameter can also add some clues onto the difference between Fe_A and Fe_B. Whatever be the Al proximity, Fe_A sites are undoubtedly more exposed while Fe_B species are more greatly interacting with the MFI framework. On the basis of the above-mentioned results any more detailed model of the sites structure is not conceivable.

From the spectra of NO adsorbed on N_2O-oxidized samples (Fig. 8a–d) we may observe that (i) the intensity of the NO bands is weakened (the effect being particularly evident on Fe–silicalite); (ii) the sites associated with the di-nitrosylic/tri-nitrosylic species (Fe_A sites) are severely affected. This result is similar to that obtained with N_2O probe titration, but the explanation is different. In the N_2O case, the intensity decrement was due to the mere presence of adsorbed oxygen filling the coordination sphere of Fe (so not allowing further N_2O insertion into the coordination sphere). On the contrary in the NO case, adsorbed oxygen on Fe_A sites (α-oxygen) readily react with NO with formation of oxidized NO_x species. The latter species (and not adsorbed oxygen) could be responsible (at least partially) for the blocking of Fe_A sites. This hypothesis is fully confirmed by the results illustrated in Fig. 9.

From this figure it can be seen that upon NO contact, besides the already documented nitrosylic contributions, bands at 2133 and at 1650 to 1550 cm^{-1} are clearly present. These bands are not ob-

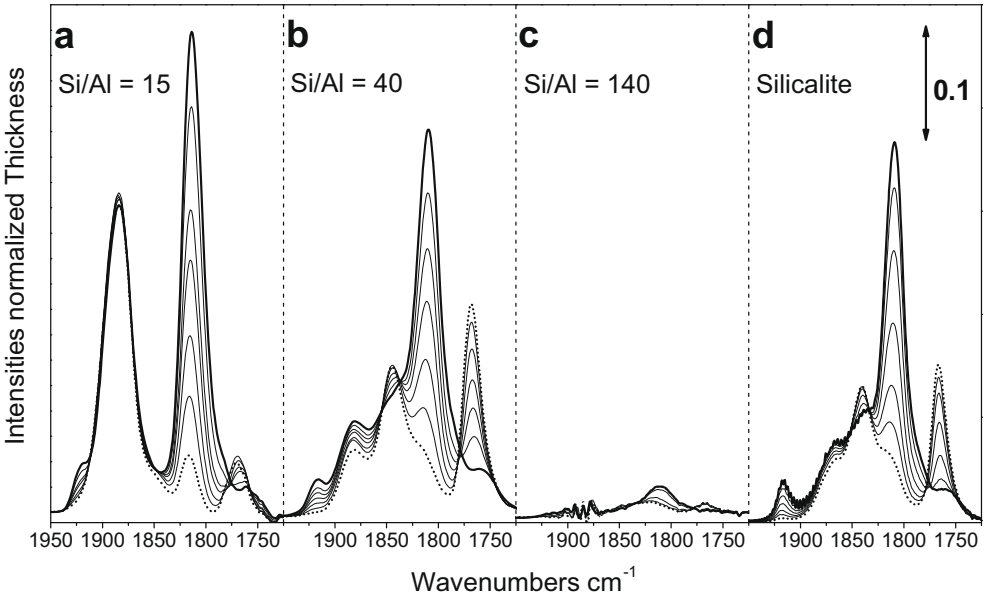

Fig. 7. FTIR spectra (background subtracted) of NO dosed at RT on (a) Fe–Z-15 (Fe 0.37 wt.%), (b) Fe–Z-40 (Fe 0.32 wt.%), (c) Fe–Z-140, and (d) Al-free Fe–S (Fe 1.0 wt.%) samples previously activated in vacuum at 773 K. Spectra were collected by reducing NO equilibrium pressure (P_{NO}) from 15 Torr (bold spectrum) to 10^{-3} Torr (dotted spectrum).

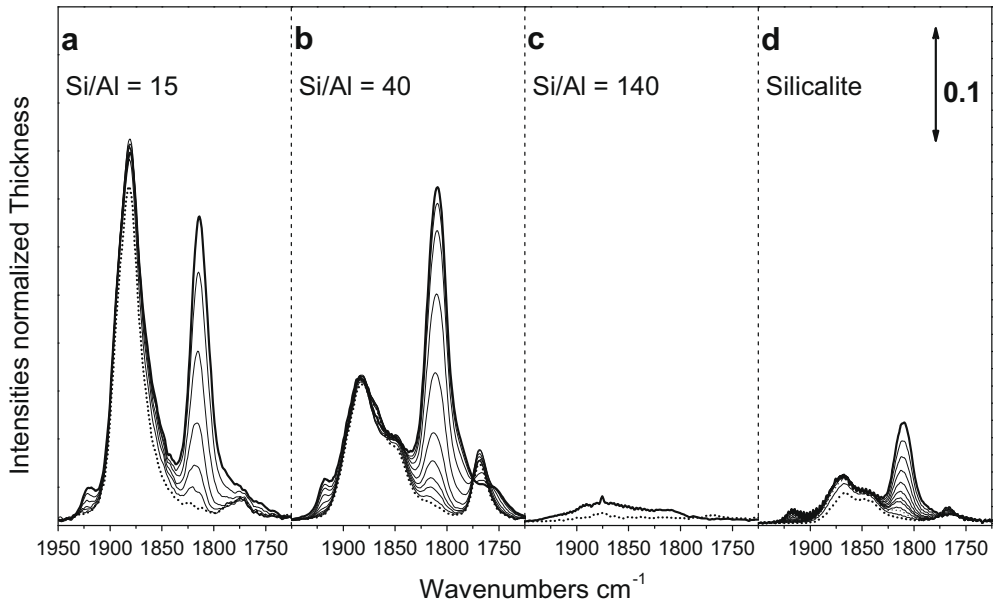

Fig. 8. FTIR spectra (background subtracted) of NO dosed at RT on (a) Fe–Z-15 (Fe 0.37 wt.%), (b) Fe–Z-40 (Fe 0.32 wt.%), (c) Fe–Z-140, and (d) Al-free Fe–S (Fe 1.0 wt.%) samples previously activated and then oxidized in N_2O atmosphere (15 Torr at 573 K). Spectra were collected by reducing NO equilibrium pressure (P_{NO}) from 15 Torr (bold spectrum) to 10^{-3} Torr (dotted spectrum).

served when a similar experiment is performed on Al-free Fe–silicalite (not shown). We hypothesize that the appearance of these bands is due to NO interaction with oxygen adsorbed on Fe_A sites (at RT) with formation of NO_2. This molecule can be directly adsorbed on iron centers with formation of $Fe^{3+}(NO_2)^-$ or, in the dimeric form (N_2O_4), disproportionate into NO^+ and NO_3^-. This hypothesis is especially consistent with the presence of the 2133 cm^{-1} band. In fact Hadjiivanov et al. [58,65,66] have observed the same band on the H–ZSM-5/NO_2 system which has been assigned (after isotopic tests) to NO^+ species. The formation of NO^+ species can be justified as follows: N_2O_4 (which is in equilibrium with NO_2) originates first NO^+ and NO_3^- [67–69] and then NO^+ readily exchanges with H^+ of H–ZSM-5 Brønsted sites with formation of adsorbed NO^+. The overall reaction scheme is

$$2NO_2 \leftrightarrow N_2O_4 \leftrightarrow NO^+ \cdots NO_3^- \quad (9)$$

$$NO^+ \cdots NO_3^- + H^+ \leftrightarrow NO^+ + HNO_3 \quad (10)$$

Of course a similar reaction sequence can occur if NO_2 is generated on Fe–ZSM-5 by reaction on NO with preadsorbed oxygen. In conclusion, the formation of NO^+ species (at 2133 cm^{-1}) at RT after NO contact with the previously oxidized Fe–ZSM-5 (by N_2O) gives indirect and convincing evidence of the presence of adsorbed oxygen and of its reactivity. From this, it also emerges that NO can not only probe Fe^{x+} sites, but also react with adsorbed species ($_*O$). This reactivity could help to understand the promoting effect of NO in N_2O decomposition. Notice that the interaction between NO and deposited O_{at} has been clearly evidenced in catalysis test, where NO promotes N_2O decomposition reaction. The presence of $Fe^{3+}(NO_2)^-$ species cannot be detected by IR because the bands of $(NO_2)^-$ occur usually in a region where the skeletal modes of the matrix absorb strongly. However, the formation of new Fe^{3+} species upon NO contact is indirectly proved by the increase of the band at 1870 cm^{-1} which is known to belong to $Fe^{3+}(NO)$ species.

About the destiny of NO_3^-, we remark that weak bands are observed in the 1650 to 1600 cm^{-1} range, which can be assigned to adsorbed nitrate species $(NO_3)^-$. These species could be located either on iron centers or on the matrix (vide infra).

On the basis of the above points, we shall compare and discuss on the spectroscopy of adsorbed NO_2 on Fe–ZSM-5, Fe–silicalite, H–ZSM-5 and silicalite.

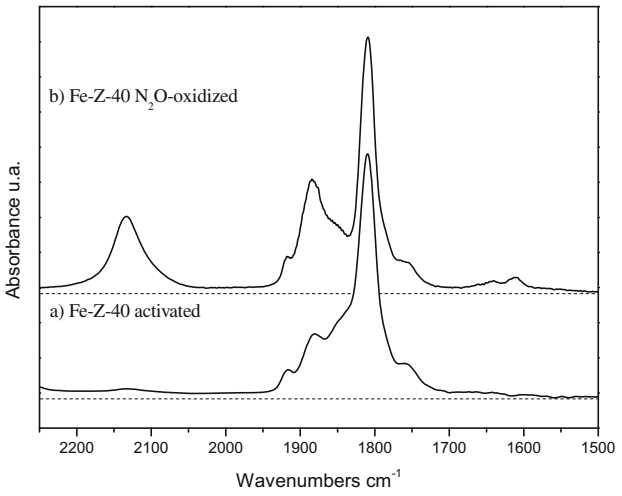

Fig. 9. FTIR spectra (background subtracted) of 15 Torr NO dosed at RT on Fe–Z-40 after activation at 773 K in He (a) and after N_2O contact at 573 K (b).

4.3. Relation between activity in N_2O abatement and active sites titration with NO and N_2O

The connection between catalysis and active sites characterization is generally not straightforward. In the present case this connection is made difficult by the heterogeneity of Fe sites on the surface and by the fact that only a fraction of them is really active. On the basis of the comparison of catalytic results of N_2O decomposition and of spectroscopic results concerning the surface sites titration with N_2O and NO obtained on the same samples (which form the main scope of the paper) it clearly emerges that low coor-

dinated Fe_A mononuclear sites are the most active in N_2O decomposition. Fe_B mononuclear sites, being characterized by a more complete coordination sphere, are less active. The same can be concluded about iron sites on Fe_xO_y clusters and Fe_2O_3 particles because the activity (calculated per Fe center) increases with dilution. The abundant presence of clustered species explains the anomalous activity and NO spectra of Fe–Z-15 sample.

4.4. Nitrogen dioxide

The spectra illustrated in Fig. 9 have shown that NO can react with adsorbed oxygen with formation of adsorbed NO_x species. To give a fully convincing assignment of the bands illustrated in Fig. 9 we have planned to investigate the spectroscopy of adsorbed NO_x species formed by direct adsorption of NO_2. This study is not only useful for the above-mentioned scope but has also general validity. In fact, the dual character of NO_2 (N_2O_4) which can generate NO^+/NO_3^- pairs allows to simultaneously probe the acid and basic sites present on the surface. In Figs. 10 and 11 the spectra of adsorbed NO_2 on silicalite, H–Z-40 (H–ZSM-5; Si/Al = 40), Fe–S, and Fe–Z-40 are illustrated.

From the results displayed in Fig. 10a (silicalite), the following can be noticed:

(a) The strong reversible peak at 1745 cm^{-1} can be assigned to the $\nu_{as}(NO_2)$ of physisorbed N_2O_4 (ν_9) (in the symmetric D_{2h} form). Weaker and tailed bands are observed at 3425, 3105, 2963, and 2628 cm^{-1} (not shown for brevity) which are also associated to the adsorbed N_2O_4 (2630 cm^{-1} ($\nu_1+\nu_{11}$), 2970 cm^{-1} ($\nu_5+\nu_{11}$), 3110 cm^{-1} ($\nu_1+\nu_9$), and 3425 cm^{-1} ($2\nu_9$)) [56]. It is known that in condensed phase or in matrix isolation conditions N_2O_4 can assume an asymmetrical configuration (planar cis/trans $ONONO_2$) characterized by very similar (although slightly lower) frequencies. In our opinion the shoulder at 1710 cm^{-1} and the distinct tails on the low frequency side of the 3105, 2963, and 2628 cm^{-1} overtones are due to the presence of the D_{2d} isomer.

(b) The weaker band at 1612 cm^{-1} is assigned to physically adsorbed NO_2 in equilibrium with N_2O_4. This assignment is confirmed by the reversible character of the band during outgassing at RT.

(c) The peak at 1658 cm^{-1}, being irreversible upon outgassing at RT, must be assigned to chemisorbed NO_x as surface nitrites or nitrates. The precise assignment of this band is not straightforward because of the huge variety of nitro, nitrito, and/or nitrato, mono and/or bidentates, chelating and/or bridging species that can be involved [57,58,70]. Usually, modes of surface NO_3^- nitrates are found in the 1650 to 1500 cm^{-1} range, while surface NO_2^- nitrites are observed around 1440 to 1100 cm^{-1} range [57,58], i.e. in a region obscured by the presence of intense modes of the siliceous MFI matrix. For this reason, the band at 1658 cm^{-1} (Fig. 10a) has to be preferentially assigned to NO_3^- nitrates species[71–73]. The involved sites are possibly the SiO,Si strained bridges formed upon high temperature dehydroxylation as the following mechanism

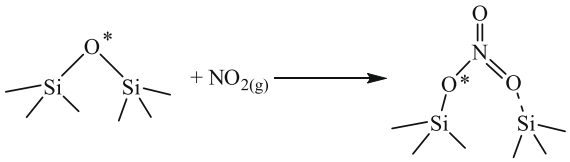

(11)

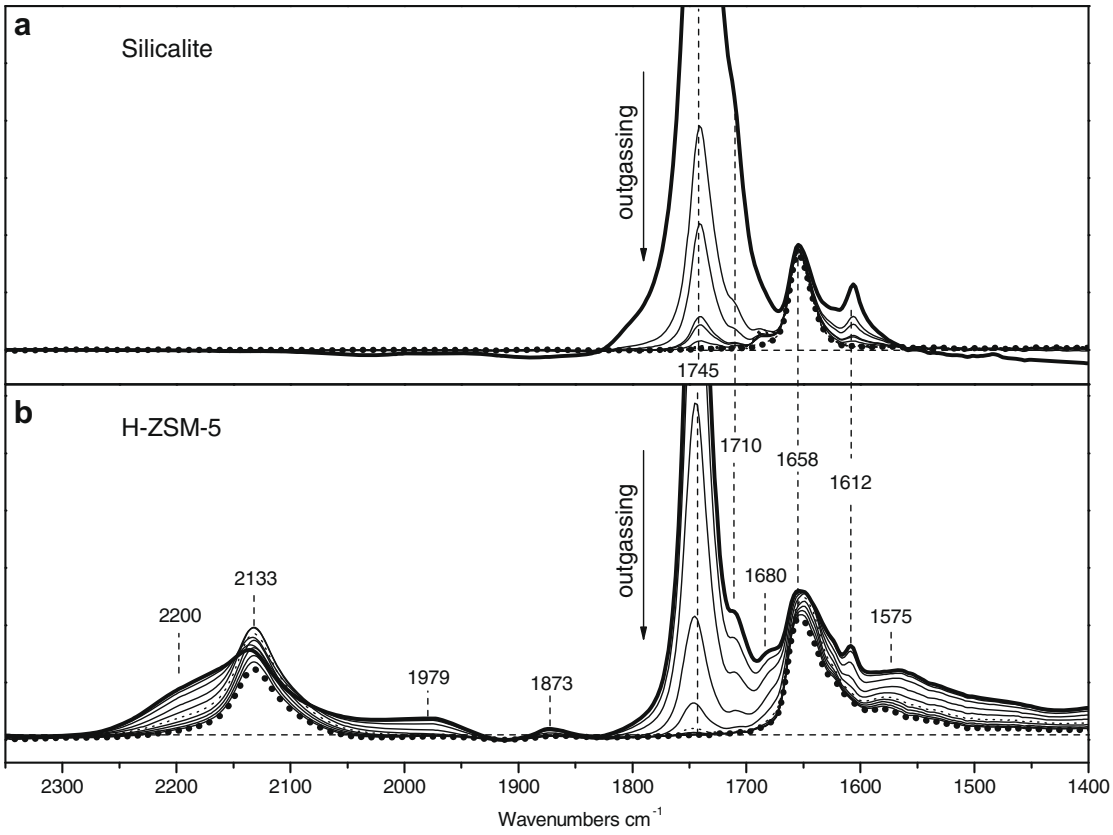

Fig. 10. Difference spectra of (a) silicalite after 10 min interaction at RT with NO_2 (bold line) and after 30 min outgassing (dotted line); (b) H–Z-40 after 10 min interaction at RT with NO_2 (bold line) and after 30 min outgassing (dotted line). Dashed line is zero level.

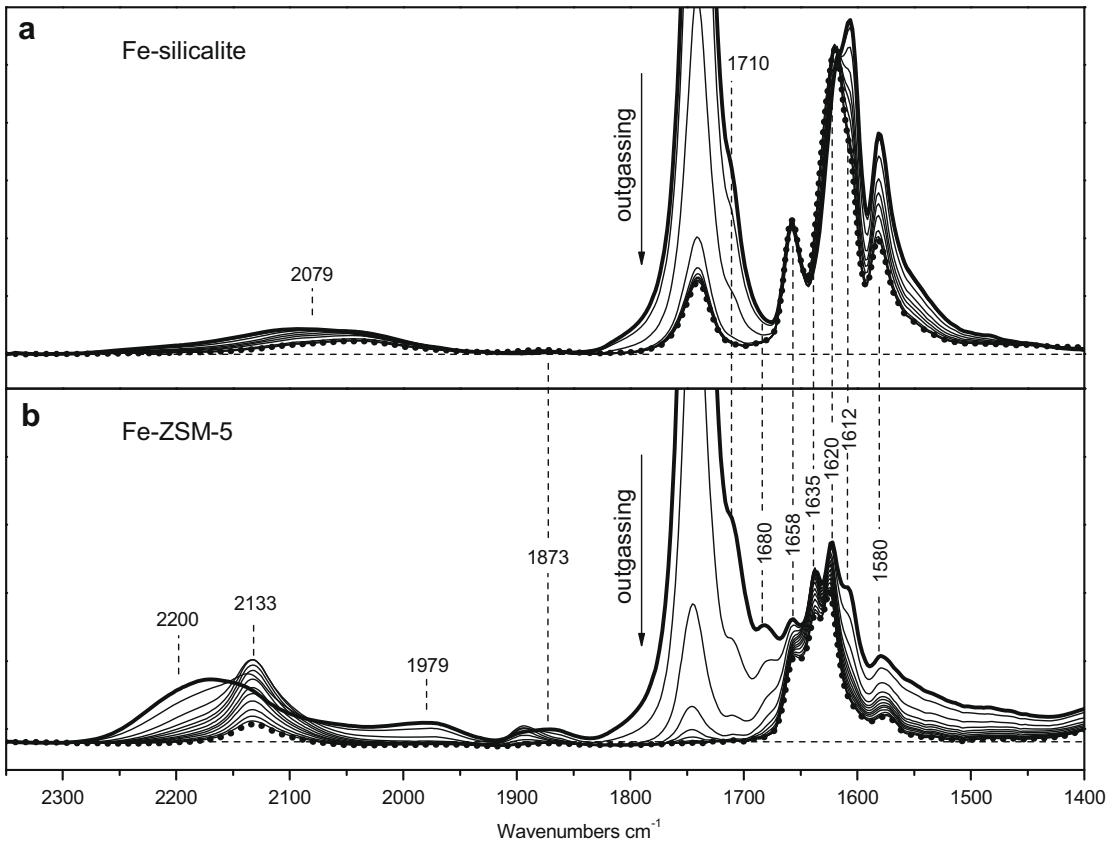

Fig. 11. Difference spectra of (a) Fe–S after 10 min interaction at RT with NO_2 (bold line) and after 30 min outgassing (dotted line); (b) Fe–Z-40 after 10 min interaction at RT with NO_2 (bold line) and after 30 min outgassing (dotted line). Dashed line is zero level.

It is a matter of fact that upon NO_2 dosage a shoulder at 910 and a peak at 896 cm^{-1} (attributed to distorted SiO*Si bridges) are strongly weakened (results not shown for brevity). It is so concluded that the pure siliceous part of the framework clearly participates in the adsorption and stabilization of NO_2. From this point and from Fig. 10b the following emerges:

(a) A band at 2133 cm^{-1} and a broad shoulder at 2200 cm^{-1} which can be attributed to the ν(NO) of NO^+ species are clearly observed (not present on silicalite). The shoulder at 2200 cm^{-1} is progressively weakened by decreasing the pressure of NO_2 (N_2O_4). This decrement is accompanied by the simultaneous increase of the peak at 2133 cm^{-1}. This effect is attributed to the destruction of a weak complex $(SiO^-Al)NO^+\cdots N_2O_4$ [58,74,75] responsible for the shoulder at 2200 cm^{-1}. This is in agreement with the observation that the band at 2200 cm^{-1} increases proportionally with the growth of the "N_2O_4 band" at 1745 cm^{-1} and disappears upon outgassing.

(b) With respect to silicalite/NO_2 system (Fig. 10a), additional bands appear at 1620 (shoulder) and 1575 cm^{-1} which can also be assigned to nitrates species. The 1620 and 1575 cm^{-1} bands are located on the top of a broad absorption band that covers the whole 1650 to 1450 cm^{-1} region. This broad feature is drastically weakened upon outgassing at RT and hence is due to neutral weakly adsorbed species such as HNO_3. The presence of weakly adsorbed HNO_3 is also demonstrated by the band at around 3400 cm^{-1} (not reported) which can be assigned to OH stretching modes of HNO_3 [55,57,76,77].

(c) Two new weak bands occur at 1979 and 1873 cm^{-1} (not observed on silicalite), these bands are not due to vibrational modes of new adsorbed species, but due to slight modification of the skeletal modes disturbed by the presence of strong adsorbates (a fact that is reflected in difference spectra) [78].

(d) Upon outgassing, molecular N_2O_4 and unreacted HNO_3 are directly desorbed, while nitrate species remains. The behavior of the NO^+ species (band at 2133 cm^{-1}) upon outgassing is quite interesting also because a fraction of these species is removed by outgassing. This decrement is associated with a proportional recover of the band due to Brønsted sites at 3610 cm^{-1} (Si(OH)Al) (not shown). The explanation of the removal of an ionic species by outgassing at RT is not straightforward. In the present case, this phenomenon can only be explained if NO^+ is replaced by H^+, following a shift to the left of the equilibrium in reaction (10), thanks to the presence of adsorbed HNO_3 in the cavities (band in 3430 to 3400 cm^{-1}range). A cooperation effect between two separate species (NO^+ and HNO_3) is here evidenced. The elimination of NO^+ is not complete because the outgassing procedure also directly removes HNO_3, a fact that does not allow the full reversibility of the process.

From the spectra obtained for Fe–silicalite (Fig. 11a), we may underline that they are very similar to those observed on silicalite. Some relevant differences are, however, observable. In particular, in the "nitrate range" two additional bands at 1620 cm^{-1} and at 1580 cm^{-1} appear. They can be attributed to new nitrate-like species presumably formed on the SiOFe bridges. Their formation

occurs immediately after NO_2 (N_2O_4) contact. The most stable species is that absorbing at 1620 cm^{-1}, while the other at 1580 cm^{-1} is half removed after 30 min outgassing. The short shift of the band from 1620 to 1612 cm^{-1} upon increasing the NO_2 pressure is likely due to the formation of labile NO_3^- (N_2O_4) complexes.

A novelty of this system is represented by the weak and broad absorption in the 2200 to 2000 cm^{-1} interval which is the typical region of NO^+. Similarly to what observed on H–ZSM-5 this absorption is consistently affected upon changing the NO_2 (N_2O_4) pressure. We can explain these results by assuming that even after activation at high temperature, a small fraction of Fe^{3+} remains in the framework position. As the presence of residual tetrahedral Fe^{3+} is necessarily associated with residual strong Brønsted acidity (Si(OH)Fe groups), the interaction with NO_2 leads to formation of NO^+ species following the usual process illustrated before. After outgassing at RT, a weak residual peak at 2080 cm^{-1} is clearly observable. This frequency is distinctly different from that of NO^+ observed on H–Z-40 and Fe–Z-40.

From the spectra reported for Fe–Z-40 (Fig. 11b) the following results emerge:

(a) The presence of the intense bands at 2200 to 2133 cm^{-1} (NO^+; similar to H–ZSM-5) indicates that strong Brønsted sites remain even after thermal treatment at 773 K. In other words while Fe goes easily into extra-framework position the same does not happen to Al.
(b) The OH stretching modes at 3610 cm^{-1} (Brønsted groups) are consumed as observed on H–ZSM-5 (not shown).
(c) A new band at 1635 cm^{-1} appears among the copious other modes already reported for Fe–silicalite and H–ZSM-5 systems. This band can be attributed to NO_3 species formed on FeO*Al sites [35,79,80].
(d) In the 950 to 850 cm^{-1} range all the T–O–T vibrational modes (including that at 935 cm^{-1}) are eroded (not shown).

The main difference between Fe–ZSM-5 and H–ZSM-5 is regarding the stability of NO^+ (2133 cm^{-1}). In fact while in H–ZSM-5 most of NO^+ is persistent upon outgassing, in Fe–ZSM-5 the nitrosonium species are nearly completely removed upon outgassing at RT. As an ionic species cannot leave the surface at RT by simply reducing the pressure of the gas phase, we have to admit that NO^+ reacts with negatively charged species to form a neutral species. From these results it is concluded that additional negative species are more abundantly formed on Fe–ZSM-5. In our opinion such species could be NO_2^- nitrites groups formed by interaction of NO_2 with iron sites that are specifically present on Fe–ZSM-5. Unfortunately, as said before, these species cannot be observed directly because they do not absorb in an available range. Despite this, we have here a further clear example of cooperative interaction between different species that are in mutual equilibrium inside a complex network involving acid and redox sites.

The resulting situation can be represented by Scheme 2.

The cooperative interaction between the different species that are in mutual equilibrium inside a complex network involving acid and redox sites is schematized. In the same scheme the reaction of adsorbed oxygen with NO and (partial) formation of the same species observed upon direct NO_2 dosage is also illustrated.

These observations can have important consequences on the interpretation of catalytic activity in N_2O decomposition of Fe–ZSM-5, a catalyst that usually is more active than Fe–silicalite. In previous review paper dealing with iron silicalite and iron ZSM-5 catalysts [31], we have stressed that the superior activity of Fe–ZSM-5 with respect to Fe–silicalite could be associated to higher dispersion and different electron density at the iron sites subsequent to the presence of Al in first or second cationic coordination spheres [31]. The presence of Brønsted centers as cooperating sites

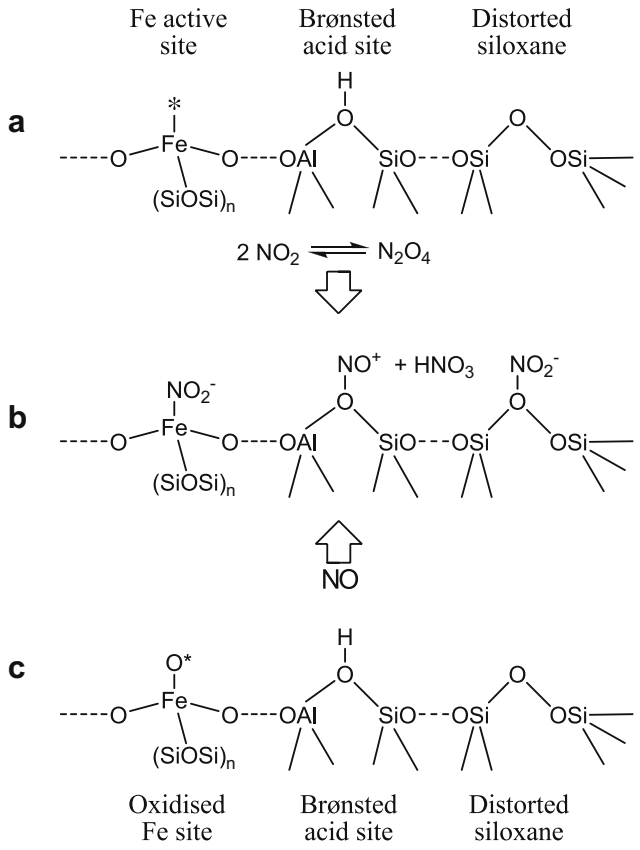

Scheme 2. Representation of the Fe–ZSM-5 catalyst surface after activation at 773 K in vacuo (a) and after oxidative treatment with N_2O at 523 K (c). The situation after NO_2 and NO adsorption at RT on vacuum treated and oxidized samples, respectively, is schematized in part (b).

was not considered. On the basis of the results obtained on the N_2O, NO_2/FeZSM-5 systems we must reconsider this statement. For instance in the case of the N_2O adsorption and decomposition mechanisms, the cooperation of Brønsted sites could be associated to their ability to give hydrogen-bonding interactions, a fact that certainly contributes to increase the concentration of N_2O in the channels of Fe–ZSM-5 with respect to Fe–silicalite. Other cooperative effects could also be hypothesized. For instance Bulushev et al. [40,41,81] have observed the evolution of NO from Fe–ZSM-5 previously contacted with N_2O decomposition at the reaction temperature. If we hypothesize that this NO comes from the decomposition of surface NO_y^- ($y = 2, 3$) species similar to those observed by direct NO_2 adsorption, the participation of Brønsted sites to the N_2O reaction could receive some comfort.

5. Conclusions

Even if at first sight the N_2O catalytic decomposition over Fe–zeolite can appear as extremely simple and stoichiometrically well defined, isotherm experiments performed at different key temperatures have highlighted the complexity of the first catalytic steps where nitrogen oxides formation cannot be ignored.

TPD tests after N_2O decomposition have demonstrated the presence of NO_2 species as products of catalysis on the surface of the Fe–MFI catalyst. Although the major part of these anionic NO_x species is adsorbed on the iron sites, the participation of SiOSi and SiO-Al distorted bridges located on Fe-free regions of the framework cannot be ignored.

The interaction of NO and N_2O probe molecules with Fe sites followed by FTIR has evidenced the presence of two families of ex-

tra-framework iron mononuclear species Fe_A and Fe_B. The difference between these two iron sites is likely due to the number of SiOSi and SiOAl ligands present in the coordination sphere of Fe(II). The Fe_A site, less coordinated to MFI zeolitic framework, appears more active and can be associated with the classical α-sites. Al vicinity is another parameter to be considered because it favors iron dispersion. Clustered species and Fe_2O_3 particles do not emerge as active participants to the N_2O decomposition reaction (under the investigated temperature conditions). Brønsted sites present in Fe–ZSM-5 interact with N_2O via hydrogen bonding with formation of stabilized complexes. These complexes are not observed on Fe–silicalite. This difference could partially explain the different activity of the two samples in the N_2O decomposition reaction.

Sites cooperation between Brønsted and iron active sites is evidenced when Fe–ZSM-5 previously oxidized with N_2O is probed with NO. In this case NO interacts directly with active oxygen species previously adsorbed (“alpha-oxygen”) on Fe_A sites with formation of NO_2 and of the associated NO^+ and NO_3^- species. The sites cooperation is also clearly demonstrated when NO_2 is directly used as a probe molecule to titrate surface sites of H–ZSM-5 and Fe–ZSM-5 zeolites.

References

[1] J. Perez-Ramirez, F. Kapteijn, K. Schoffel, J.A. Moulijn, Applied Catalysis B – Environmental 44 (2003) 117–151.
[2] P.M. Vitousek, J.D. Aber, R.W. Howarth, G.E. Likens, P.A. Matson, D.W. Schindler, W.H. Schlesinger, D.G. Tilman, Ecological Applications 7 (1997) 737–750.
[3] M.H. Thiemens, W.C. Trogler, Science 251 (1991) 932–934.
[4] R.W. van den Brink, S. Booneveld, M. Verhaak, F.A. de Bruijn, Catalysis Today 75 (2002) 227–232.
[5] A.N. Hayhurst, A.D. Lawrence, Progress in Energy and Combustion Science 18 (1992) 529–552.
[6] M.A. Wojtowicz, J.R. Pels, J.A. Moulijn, Fuel Processing Technology 34 (1993) 1–71.
[7] Y.J. Li, J.N. Armor, Applied Catalysis B – Environmental 1 (1992) L21–L29.
[8] M.A. Pena, J.L.G. Fierro, Chemical Reviews 101 (2001) 1981–2017.
[9] K. Yuzaki, T. Yarimizu, K. Aoyagi, S. Ito, K. Kunimori, Catalysis Today 45 (1998) 129–134.
[10] G.I. Panov, V.I. Sobolev, A.S. Kharitonov, Journal of Molecular Catalysis 61 (1990) 85–97.
[11] G.I. Panov, G.A. Sheveleva, A.S. Kharitonov, V.N. Romannikov, L.A. Vostrikova, Applied Catalysis A – General 82 (1992) 31–36.
[12] E. Hensen, Q.J. Zhu, P.H. Liu, K.J. Chao, R. van Santen, Journal of Catalysis 226 (2004) 466–470.
[13] K.Q. Sun, H. Xia, E. Hensen, R. van Santen, C. Li, Journal of Catalysis 238 (2006) 186–195.
[14] Y. Li, Z.C. Feng, H.C. Xin, F.T. Fan, J. Zhang, P. Magusin, E.J.M. Hensen, R.A. van Santen, Q.H. Yang, C. Li, Journal of Physical Chemistry B 110 (2006) 26114–26121.
[15] G.D. Pirngruber, M. Luechinger, P.K. Roy, A. Cecchetto, P. Smirniotis, Journal of Catalysis 224 (2004) 429–440.
[16] J. Perez-Ramirez, F. Kapteijn, A. Bruckner, Journal of Catalysis 218 (2003) 234–238.
[17] E.V. Kondratenko, J. Perez-Ramirez, Journal of Physical Chemistry B 110 (2006) 22586–22595.
[18] A. Heyden, N. Hansen, A.T. Bell, F.J. Keil, Journal of Physical Chemistry B 110 (2006) 17096–17114.
[19] I. Melian-Cabrera, S. Espinosa, J.C. Groen, B. van de Linden, F. Kapteijn, J.A. Moulijn, Journal of Catalysis 238 (2006) 250–259.
[20] G.D. Pirngruber, P.K. Roy, Catalysis Today 110 (2005) 199–210.
[21] A. Heyden, B. Peters, A.T. Bell, F.J. Keil, Journal of Physical Chemistry B 109 (2005) 4801–4804.
[22] I. Yuranov, D.A. Bulushev, A. Renken, L. Kiwi-Minsker, Journal of Catalysis 227 (2004) 138–147.
[23] G. Berlier, C. Prestipino, M. Rivallan, S. Bordiga, C. Lamberti, A. Zecchina, Journal of Physical Chemistry B 109 (2005).
[24] E.V. Kondratenko, J. Perez-Ramirez, Applied Catalysis B – Environmental 64 (2006) 35–41.
[25] L. Kiwi-Minsker, D.A. Bulushev, A. Renken, Journal of Catalysis 219 (2003) 273–285.
[26] A. Ates, A. Reitzmann, Chemical Engineering Journal 134 (2007) 218–227.
[27] A. Heyden, B. Peters, A.T. Bell, F.J. Keil, Journal of Physical Chemistry B 109 (2005) 1857–1873.
[28] G. Yang, D. Zhou, X. Liu, X. Han, X. Bao, Journal of Molecular Structure 797 (2006) 131–139.
[29] P.M. Esteves, B. Louis, Journal of Physical Chemistry B 110 (2006) 16793–16800.
[30] S. Perathoner, F. Pino, G. Centi, G. Giordano, A. Katovic, J.B. Nagy, K. Lazar, P. Fejes, Impact of Zeolites and Other Porous Materials on the New Technologies at the Beginning of the New Millennium, Pts. A and B, Elsevier Science Bv., Amsterdam, 2002, pp. 503–510.
[31] A. Zecchina, M. Rivallan, G. Berlier, C. Lamberti, G. Ricchiardi, Phys. Chem. Chem. Phys. 9 (2007) 3483–3499.
[32] N. Hansen, A. Heyden, A.T. Bell, F.J. Keil, Journal of Physical Chemistry C 111 (2007) 2092–2101.
[33] G. Grubert, M.J. Hudson, R.W. Joyner, M. Stockenhuber, Journal of Catalysis 196 (2000) 126–133.
[34] G. Mul, J. Perez-Ramirez, F. Kapteijn, J.A. Moulijn, Catalysis Letters 77 (2001) 7–13.
[35] G. Mul, J. Perez-Ramirez, F. Kapteijn, J.A. Moulijn, Catalysis Letters 80 (2002) 129–138.
[36] J. Perez-Ramirez, F. Kapteijn, G. Mul, J.A. Moulijn, Journal of Catalysis 208 (2002) 211–223.
[37] C.M. Sang, B.H. Kim, C.R.F. Lund, Journal of Physical Chemistry B 109 (2005) 2295–2301.
[38] J. Novakova, Z. Sobalik, Catalysis Letters 105 (2005) 169–177.
[39] J. Novakova, Z. Sobalik, Catalysis Letters 111 (2006) 195–202.
[40] D.A. Bulushev, A. Renken, L. Kiwi-Minsker, Journal of Physical Chemistry B 110 (2006) 305–312.
[41] D.A. Bulushev, A. Renken, L. Kiwi-Minsker, Journal of Physical Chemistry B 110 (2006) 10691–10700.
[42] B. Wichterlova, Z. Sobalik, J. Dedecek, Applied Catalysis B – Environmental 41 (2003) 97–114.
[43] E. Groppo, C. Lamberti, S. Bordiga, G. Spoto, A. Zecchina, Chemical Reviews 105 (2005) 115–183.
[44] E. Groppo, C. Lamberti, G. Spoto, S. Bordiga, G. Magnacca, A. Zecchina, Journal of Catalysis 236 (2005) 233–244.
[45] M.T. Nechita, G. Berlier, G. Ricchiardi, S. Bordiga, A. Zecchina, Catalysis Letters 103 (2005) 33–41.
[46] P. Ratnasamy, R. Kumar, Catalysis Today 9 (1991) 329–416.
[47] B.R. Wood, J.A. Reimer, A.G. Bell, Journal of Catalysis 209 (2002) 151–158.
[48] J.F. Jia, Q. Sun, B. Wen, L.X. Chen, W.M.H. Sachtler, Catalysis Letters 82 (2002) 7–11.
[49] Q. Zhu, B.L. Mojet, R.A.J. Janssen, E.J.M. Hensen, J. van Grondelle, P. Magusin, R.A. van Santen, Catalysis Letters 81 (2002) 205–212.
[50] P.K. Roy, G.D. Pirngruber, Journal of Catalysis 227 (2004) 164–174.
[51] M.N. Debbagh, A. Bueno-Lopez, C.S.M. de Lecea, J. Perez-Ramirez, Applied Catalysis A – General 327 (2007) 66–72.
[52] J. Perez-Ramirez, F. Kapteijn, J.C. Groen, A. Domenech, G. Mul, J.A. Moulijn, Journal of Catalysis 214 (2003) 33–45.
[53] F. Kapteijn, G. Marban, J. RodriguezMirasol, J.A. Moulijn, Journal of Catalysis 167 (1997) 256–265.
[54] L. Kiwi-Minsker, D.A. Bulushev, A. Renken, Catalysis Today 110 (2005) 191–198.
[55] J. Laane, J.R. Ohlsen, Progress in Inorganic Chemistry 28 (1986) 465.
[56] G. Herzberg, 2: Infrared and Raman Spectra of Polyatomic Molecules, D. Van Nostrand Reinhold, Inc., New York, 1945.
[57] K. Nakamoto, Infrared and Raman Spectra of Inorganic and Coordination Compounds, Wiley and Sons, New York, 1970.
[58] K.I. Hadjiivanov, Catalysis Reviews – Science and Engineering 42 (2000) 71–144.
[59] L.J. Lobree, I.C. Hwang, J.A. Reimer, A.T. Bell, Catalysis Letters 63 (1999) 233–240.
[60] G. Spoto, A. Zecchina, G. Berlier, S. Bordiga, M.G. Clerici, L. Basini, Journal of Molecular Catalysis A – Chemical 158 (2000) 107–114.
[61] G. Berlier, G. Ricchiardi, S. Bordiga, A. Zecchina, Journal of Catalysis 229 (2005) 127–135.
[62] G. Berlier, G. Spoto, G. Ricchiardi, S. Bordiga, C. Lamberti, A. Zecchina, Journal of Molecular Catalysis A – Chemical 182 (2002) 359–366.
[63] L.J. Lobree, I.C. Hwang, J.A. Reimer, A.T. Bell, Journal of Catalysis 186 (1999) 242–253.
[64] M. Lezcano, V.I. Kovalchuk, J.L. d'Itri, Kinetics and Catalysis 42 (2001) 104–111.
[65] K. Hadjiivanov, J. Saussey, J.L. Freysz, J.C. Lavalley, Catalysis Letters 52 (1998) 103–108.
[66] A. Penkova, K. Hadjiivanov, M. Mihaylov, M. Daturi, J. Saussey, J.C. Lavalley, Langmuir 20 (2004) 5425–5431.
[67] A.M. Vos, P. Mignon, P. Geerlings, F. Thibault-Starzyk, R.A. Schoonheydt, Microporous and Mesoporous Materials 90 (2006) 370–376.
[68] J. Szanyi, J.H. Kwak, R.A. Moline, C.H.F. Peden, Physical Chemistry Chemical Physics 5 (2003) 4045–4051.
[69] I. Perdana, D. Creaser, O. Ohrman, J. Hedlund, Applied Catalysis B – Environmental 72 (2007) 82–91.
[70] V.H. Grassian, International Reviews in Physical Chemistry 20 (2001) 467–548.
[71] T. Venkov, K. Hadjiivanov, D. Klissurski, Physical Chemistry Chemical Physics 4 (2002) 2443–2448.
[72] J. Szanyi, J.H. Kwak, R.J. Chimentao, C.H.F. Peden, Journal of Physical Chemistry C 111 (2007) 2661–2669.
[73] C. Paze, G. Gubitosa, S.O. Giacone, G. Spoto, F. Xamena, A. Zecchina, Topics in Catalysis 30–31 (2004) 169–175.
[74] Q. Sun, Z.X. Gao, H.Y. Chen, W.M.H. Sachtler, Journal of Catalysis 201 (2001) 89–99.

[75] Z.X. Gao, S. Qi, W.M.H. Sachtler, Applied Catalysis B – Environmental 33 (2001) 9–23.
[76] C. Borensen, U. Kirchner, V. Scheer, R. Vogt, R. Zellner, Journal of Physical Chemistry A 104 (2000) 5036–5045.
[77] K. Hadjiivanov, Catalysis Letters 68 (2000) 157–161.
[78] A. Zecchina, F. Geobaldo, G. Spoto, S. Bordiga, G. Ricchiardi, R. Buzzoni, G. Petrini, Journal of Physical Chemistry 100 (1996) 16584–16599.
[79] E.J.M. Hensen, Q. Zhu, R.A.J. Janssen, P. Magusin, P.J. Kooyman, R.A. van Santen, Journal of Catalysis 233 (2005) 123–135.
[80] Q. Yu, X.P. Wang, N. Xing, H.L. Yang, S.X. Zhang, Journal of Catalysis 245 (2007) 124–132.
[81] E.M. El-Malki, R.A. van Santen, W.M.H. Sachtler, Journal of Catalysis 196 (2000) 212–223.